Date of submission: 25/07/2022

Qualitative comparison of the pre-processing pipelines of the inferior cerebellar peduncle in pre-operative paediatric oncology data

Major Research Project Report

Darja Rakitina

University Medical Centre Utrecht (UMCU), Imaging Division

Utrecht

The Netherlands

d.rakitina@umcutrecht.uu.nl

ABSTRACT Cerebellar mutism syndrome (CMS) arises in some patients after the surgical removal of posterior fossa tumours. The complications include speech retardation, emotional lability, various mobility impairments and developmental delays. Even though this form of cancer makes up a big part of the mortality rates in paediatric oncology, the evidence for what causes the CMS complication is still generally unknown.

The clinical interest in cerebellar investigation relies onto differentiating anatomical properties influencing CMS pathogenesis. Diffusion-weighted imaging (DWI) of a cerebellar region can help to identify the areas, which contribute to the development of CMS. Being based on the principle of diffusion anisotropy, this technique can provide an overview of the connectivity and volumes of white matter regions in the brain. After minimising artefacts and performing the registration, a cerebellar region can be investigated with fiber tractography. The tract of interest, which in the case of this project is the inferior cerebellar peduncle (ICP), is segmented. Then parameters like mean diffusivity (MD) and fractional anisotropy (FA) can be acquired as quantitative markers of white matter microstructural differences. Along with the segmented tract profiles, obtained FA and MD can be compared between the two groups: patients who developed CMS and who did not. Identifying the regions that contribute to the development of CMS can be used when considering the risks of CMS development in surgical planning.

This report compares two pre-processing pipelines, aiming to choose the more suitable one considering the presence of the tumour. It discusses the challenges associated with the visualisation of tracts near the cerebellum and sources of errors and proposes improvements that could be considered in terms of the future development of the project. It also describes the outcomes of a deterministic tractography method used for segmentation of the inferior cerebellar peduncle.

The study concluded that the FSL pre-processing pipeline resulted in more visual improvements in a particular cohort than the pre-processing performed in ExploreDTI. However, the reliability of tractography results was lowered due to the presence of remaining artefacts. Therefore, further pipeline development is required before the segmentation of ICP and assessment of tractography parameters can make it possible to discover reasons for CMS development.

LAYMANS SUMMARY

Posterior fossa brain tumours make up about half of all paediatric oncology cases. Some of these result in cerebellar mutism syndrome (CMS), which induces various speech and movement problems as well as emotional lability and developmental delays. There is a transient type of this syndrome, which resolves within 7-10 days, although most cases leave permanent damage. Posterior fossa tumours are usually removed surgically without the need for chemotherapy and radiological treatments. The clinical concern is to find out what contributes to the development of this syndrome in some patients, so that the damage of white matter tracts, which could contribute to CMS development, can be surgically avoided. Moreover, the risk of CMS development can be noticed and considered during surgical planning.

The problem starts here: the cerebellum is a tricky part of the brain to visualise. Cerebellar functional units are comparatively small and densely allocated. Even in healthy individuals, this part of the brain has not been studied enough. It has been previously "scientifically neglected" and is not included in most brain atlases because it is hard to visualise and, therefore, map the cerebellum. Brain atlases are images that contain anatomical or physiological information about the brain, usually based on the scans of healthy individuals. These are used as a reference in brain research and are required as a baseline when studying pathologies, like CMS. Therefore, until this day this part of the brain holds a lot of mysteries. For example, it is not directly connected to the known speech centres, but still seems to contribute to the speech processing features.

Investigation of the mutism of cerebellar origin in vivo can be done with diffusion-weighted imaging (DWI). This technique allows looking into the connectivity of different brain areas as well as the volumes of white matter regions. Based on the random water molecule movement, DWI captures the main diffusivity trends. They are characterised by fractional anisotropy (FA) and mean diffusivity (MD). Due to the differences in density of different tissue types, the diffusion coefficient varies. For instance, FA of 0 corresponds to isotropic diffusion, meaning the same in all directions. In anisotropic diffusion, molecules tend to have a clear preference in one direction. Based on these parameters, the diffusion model is estimated. The diffusion weighted images can also be overlapped with a normal MRI scan, which is used as a reference for diffusion data registration.

This project focuses on the white matter tracts of the inferior cerebellar peduncle (ICP). Mainly because it results in a neuronal output from the cerebellum to the parts that contribute to the linguistic brain centres, while the other two peduncles are input to the cerebellum. Different pre-processing pipelines were tested and compared in order to find the best technique for processing data of this kind. Diffusion imaging tractography was performed after, focusing on a segmentation of the ICP. A total of 48 pre-operative MRI scans were analysed when comparing the two pre-processing pipelines (ExploreDTI and FSL) in terms of this project. For 14 of these patients, the tractography of the inferior cerebellar peduncle was attempted. It allowed to visually evaluate the quality of the pre-processing steps and highlight the necessary improvements for further research.

INTRODUCTION

Cerebellar Mutism Syndrome (CMS) arises in paediatric oncology patients mainly after cranial posterior fossa tumour removal surgery. However, not all patients develop CMS after the procedure. About 24% of medulloblastoma patients have been reported to develop CMS. The post-surgical impairments lead to a delay in several neurocognitive functions, which affect patients' life through emotional incontinence and lability, reduced processing speed, various movement and mobility impairments, speech retardation, attention deficit etc. [1]. Interestingly, these problems are not primarily associated with the part of the brain, which is being surgically altered. The leading risk factors are thought to be the proximity of the tumour towards the midline and the brainstem involvement.

Investigation of the mutism of cerebellar origin in vivo can be done with diffusion magnetic resonance imaging (dMRI). Diffusion imaging is based on the Brownian motion, which is a result of constant random water molecule movement. The assessment of brain tissue connectivity or white matter volumes is usually done with the following diffusion parameters: fractional anisotropy (FA), mean diffusivity (MD), axial diffusivity and radial diffusivity (RD). More information about the dMRI principles can be found in Appendix A.

Allocated in the posterior cranial fossa, the cerebellum is connected to the medulla oblongata by the cerebellar inferior peduncle, as it can be seen in Figure 1 [2]. A previously conducted study [1] has shown that FA drops in patients with CMS as compared with non-CMS patients undergoing a similar operation. Preoperative MRI scans were used to characterize tumour features, while postoperative MRI and dMRI were obtained to define operative injury and tract-based differences in FA of water molecules. The findings of the study suggest that the FA of water diffusion was decreased by functional disruption of the WM bundles and is related to the abnormal posterior fossa syndrome neurobehavioral symptoms.

Other previously proposed theories suggested CMS occurs as a result of bilateral damage to the connection of the superior cerebellar peduncle (SCP) and the dentate-rubro-thalamic (DTR) tract or dentate nucleus [3]. This has a negative impact on the overall volume of the WM in the frontocerebellar region, which is a speech center of the brain [3, 4, 5].

The defined and united pathogenesis for the CMS remains unclear. There also isn't enough evidence about the long-term development of the syndrome. This is due to the absence of a consolidated monitoring protocol and the complexity of the necessary assessment to perform at the post-surgical checkpoints. However, the growing amount of prospective and retrospective studies arising in the past few years provides a better perspective into the cerebellar functions and theories on the origination of the CMS [4]. There is also evidence suggesting that retrospective studies report a lower incidence of the CMS, while the general occurrence has an upward trend [1].

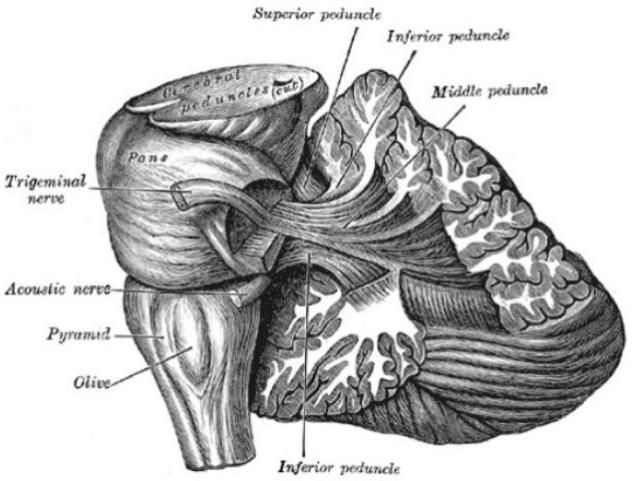

FIGURE 1. The defined and united pathogenesis for the CMS remains unclear. There also isn't enough evidence about the long-term development of the syndrome. This is due to the absence of a consolidated monitoring protocol and the Anatomical Structure of Cerebellar Peduncles [6].

The study performed by Leitner Y. et al has segmented all three cerebellar peduncles (middle, two inferior and two posterior) in 19 healthy infant and adolescent patients of the ages 9-17 [8]. With the placement of 30 equidistant points, they obtained tract profiles, when searching for age-dependent deviations in axial, radial, mean diffusivities and FA. The diffusion measures of generated tract profiles do not confirm any systematic alterations and show consistent variation patterns among individuals. However, tractography was performed on a comparatively small cohort to provide a fair judgement on how the tract variability could influence neurocognitive and neuromotor development. The description of seed point allocation, as well as obtained tractography measures, can now be used as a reference for the investigation of cerebellar pathologies in infants and adolescents (Figure 2).

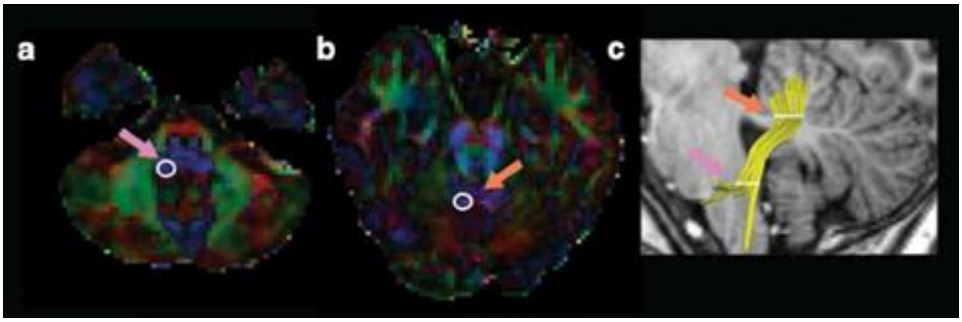

FIGURE 2. Allocation of ROIs in healthy adolescent brain for left inferior cerebellar peduncle (ICP) segmentation, reference from Y. Leither et al. Here used as a seedpoint allocation reference for the segmentation of (ICP) in tractography step [8].
Figure 2a is a red-green-blue (RGB) colour map of coronal view, x-direction. Pink arrow in Figure 2a indicates a placement of the first seed point.
Figure 2b is axial view, z-direction. Orange arrow in Figure 2b is a location of the second seed point placement.
Figure 2c shows segmented ICP in the left hemisphere (yellow structure).

This work focuses on analysing the inferior cerebellar peduncle (ICP). It is one of the three cerebellar peduncle tracks. This area was chosen as it's the expected neuronal output to the linguistic centers in the brain. DMRI was selected as a tool for the investigation, as it allows visualization of the locations and orientations of subcortical WM tracts in vivo. The previous studies relied on dMRI to track the post-surgical changes in volumes of the brain structures, like reductions in FA and MD [9]. However, the focus of this project is on finding the optimal pre-processing pipeline for pre-operational scans, which would not compromise the tractography investigation. The presence of a tumour is a high source of variability, which makes it challenging to find a suitable pre-processing pipeline. Investigation of a cerebellar region with dMRI, relying on measurements of FA and MD, can potentially identify qualities in pre-operational scans that might be leading to the development of the CMS. That would allow to learn about microstructural differences that distinguish patient groups with post-surgical CMS and non-CMS development. With a sufficient amount of evidence, this could help to highlight high-risk regions and this information can be advantageous in consideration of risks in surgical planning.

METHODS

0. Experimental Data Description

This study is based on at a dataset provided by the Princes Maxima Center for pediatric oncology (Utrecht, The Netherlands). It contains 148 patient records, of which 48 were tested in terms of this project and 14 of which were used in the final analysis stages of the project. That included FSL pre-processing and ExploreDTI tractography. The rest of the samples have been excluded due to the absence of diffusion data or a T1-weighted scans. The T1-weighted image was used as an anatomical reference during an image registration step.

The majority (31) of the scans has been acquired with 16 b-values of 800 s/mm^2, while the other part (14) of the cohort was acquired with 17 b-values of 1000 s/mm^2. Additionally, three samples out of the 48, have been acquired with 2 b-values: 1000 & 2000 s/mm^2. In those cases, only the b-value of 1000 s/mm^2 was used to reduce the variability of data. Echo times (TE) in the cohort varied between 82-86 milliseconds, with prevalence (6 patients out of 14) being acquired with TE = 83 miliseconds.

Out of 14 patient records, which have been included in the final pipeline, only 2 had a record of CMS development. The gender was known for 12 patients, being 8 male and 4 female, where CMS presence was 1 in each gender group.

It was decided to analyse only the first scan, which is a pre-operational scan, in all of the data sets, due to the storage limitations and time constraints of the current project. In order to minimise sources of variability, the subset with matching acquisition parameters was selected. For the same reason and to reach a more standardised input, only one b-value was used in the case of files that were acquired with more.

1. Pre-Processing

The comparison of the pre-processing pipelines done with ExploreDTI and FSL tools was performed to find out which one is more suitable for the cohort. The main differences between approaches are in the eddy current modelling algorithms. The FSL eddy current correction function has an option to perform slice-to-volume registration with an outlier replacement. This is hypothesised to have an overall advantage over the pipeline performed in ExploreDTI.

A. ExploreDTI

Patient data was initially received in a DICOM format, so a conversion to a 4D file format was the first step. It was done with the dcm2niix tool, which is a part of MRIcron (v1.0.20190902) package [15]. It extracts the information about diffusion directions from the DICOM file's header and creates *.bval and *.bvec files, which contain b-value and b-vector information, respectively. For the processing in

ExploreDTI, the information from these two files should be combined into a *.txt file that contains diffusion gradient settings.

While working in ExploreDTI, it is important to keep file names clear and consistent. This way it is easier to track back the performed steps. After the DICOM to nifti conversion step, the files were renamed for convenience. The input was standardised to perform analysis on multiple datasets in parallel. Most of the functions also suggest a little alteration to the input file names, when producing output.

Signal drift correction is a necessary next step. It is performed to correct for acquisition-related artefacts – the intensity drift of the signal across different diffusion MRI volumes [17]. The tendency of change is estimated and applied as a multiplicative factor across the dataset for correction. It results in an updated nifti and *.txt files, which are then used to create a *.mat file for visual inspection of improvements. Visual inspection is, generally, a good measure of progress after every performed step when working with images.

The next step was the creation of a *.mat file which is required to check if the scans are flipped correctly - according to the neurological or radiological convention (left/right flip). The conventional flip of the diffusion directions was ensured at this step. The spatial and diffusion coordinate system match is automatically calculated and necessary changes are suggested by ExploreDTI tool [15]. For a particular dataset, x and y gradient orientations were permuted and the sign of z component flipped (gradient component permutations: y, x, z; flip of the sign of gradient components: x y -z).

After the creation of a *.mat file, the residual maps were checked, an example can be seen in Figure 3. The output was produced with the use of the inbuilt ExploreDTI function that provides an insight into data quality by producing outlier profiles, residual maps and graphs with absolute residual model errors.

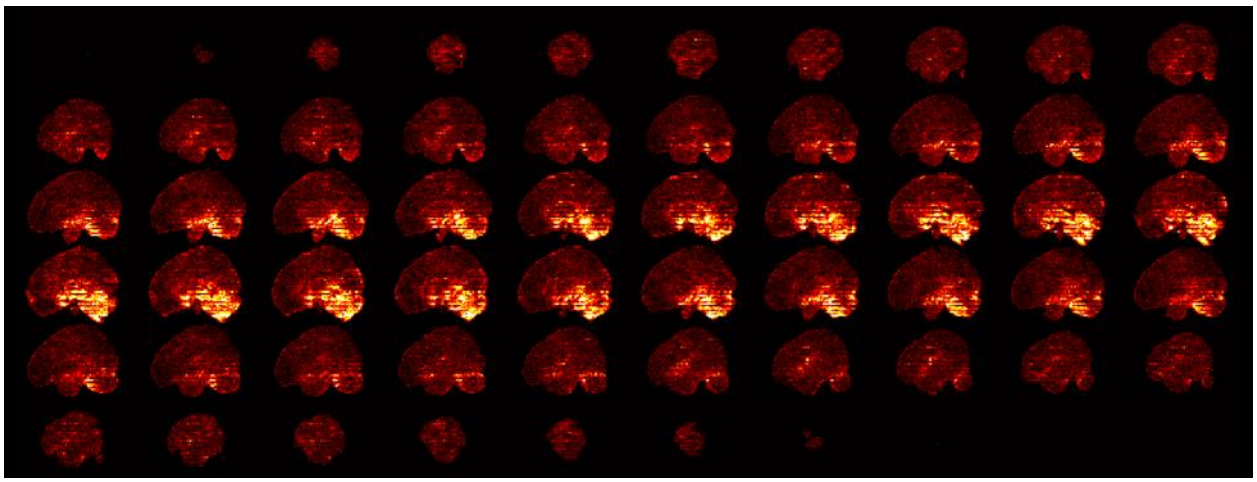

FIGURE 3. **Data quality summary, sagittal view via the residual map. Raw, no pre-processing.**

The accuracy of the diffusion data is easily influenced by the subject motion, physiological movements and artefacts produced during the acquisition process. It is therefore necessary to spatially realign the b-matrix, preserving the diffusion gradient orientation information. Otherwise, it could implicate the results in a form of potential shifting, scaling, and shearing phase encoding artefacts [18]. Subject motion and epi distortion correction was done as pre-processing step to improve the registration of the DTI volumes to T1-weighted MRI scans [19].

B. FSL

The flow of the pre-processing pipeline performed in FSL is visualised in Figure 4. Firstly, the default functionality of a brain extraction tool (BET) was applied to the diffusion data. The output from this step was used as a mask when running eddy current corrections. This was also done to speed up further processing steps by removing the non-brain tissue from the scans. Visual inspection was performed individually per patient upon completion to ensure the preservation of the necessary brain parts. The default BET setting of the fractional intensity threshold was varied between 0.3 and 0.45, where bigger values result in smaller brain outline estimates.

BET was also applied to the T1-weighted MRI scan to create a mask for *epi_reg*, which is a registration function. The output mask contained removed skull and residual soft tissues and extracted brain volumes.

The next step was correcting eddy current induced distortions and misalignment due to subject motion. The diffusion mask generated in the previous step was used for this. Some additional parameter files were created to fill in the gaps that would allow to still use this FSL tool. The actual numbers inserted did not matter with the current protocol, therefore it was not an additional source of variability. Because the patient data that was used in the analysis stages of this project had the same settings (number of non-DWI and DWI, volumes and b-values). It would have had an influence with the variation of EPI readout (like phase encoding direction); however, it was not altered here [21]. This is due to the lack of information about acquisition procedures and settings. Code for the commands to apply *eddy* function can be found in Appendix B, as the rest of the necessary information to duplicate the performance of the FSL pre-processing pipeline.

An important detail in the settings of *eddy* was to ensure it performs a slice to volume registration [22, 23]. This was applied by tuning in *mporder* function, which improves the quality of the acquired diffusion data by intra-volume movement correction [24]. The principle of this algorithm is based upon the assumption of the subject remaining motionless while the volume is being acquired and movement happening between the last acquired slice and the first slice of new volume [24]. Solving the issue of signal dropout is done by the outlier replacement (*repo*l) algorithm [26]. It detects the slice, which happens to have a coinciding motion with the scanning sequence. And then it patches it with a prediction of the gaussian process [23]. The default setting is removal of slices, where the brightness is four standard deviations lower than average intensity [26]. Additionally, niter option is applied, which speeds up the *eddy* processing by running it for multiple iterations [24]. The default setting was applied here, which is 5 iterations.

Further information on the abovementioned tools can be found on the official FSL webpage [27]. As part of this pipeline, newly produced *.bvec and nifti files were of interest for further processing steps.

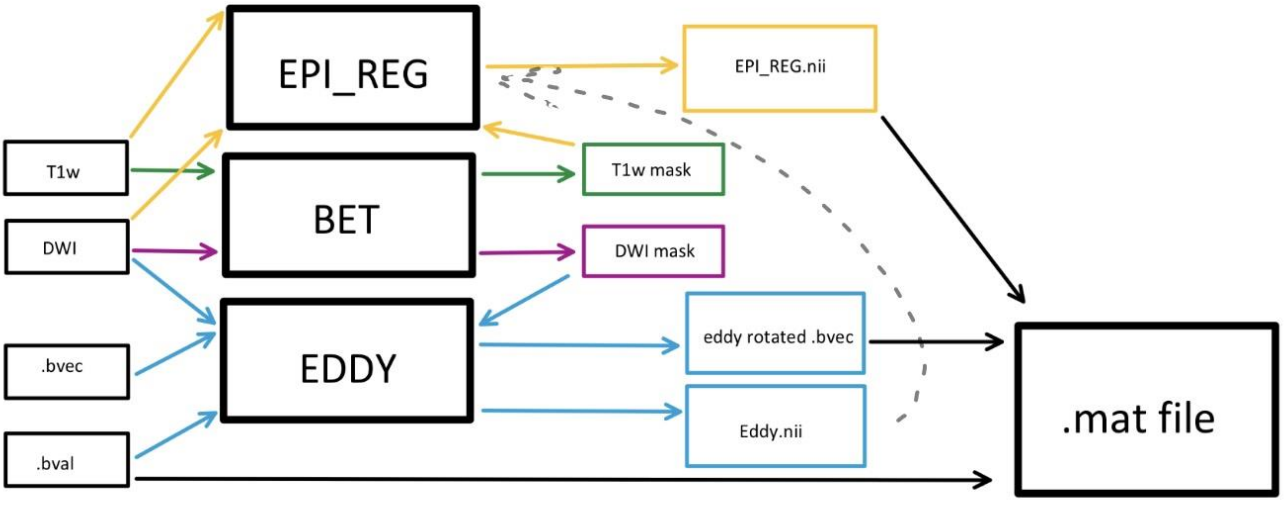

FIGURE 4. FSL Methods Schematical Overview.
Left column from above-down as follows: T1-weighted MRI scan, diffusion MRI scan, files containing b-vectors and b-values Three main functions used within the FSL framework: *epi_reg*, BET and *eddy*.
Yellow arrows connect files to *epi_reg* function, blue arrows connect files to *eddy* function,
The dashed line indicates that the resulting *eddy* function's output is used as an input for *epi_reg* function.
The black arrows indicate files used for *.mat file creation, which is used for tractography.

This *epi_reg* step performs a registration of diffusion data to the T1-weighted anatomical image. The default settings have been used without additional parameter alterations mainly due to the lack of information about the acquisition (Appendix B).

This function uses a T1-weighted scan, a T1-weighted mask produced with BET and a nifti file, which was an output from *eddy*. This registration is based on a principle of differentiating white/grey matter boundary and that is why this function also produces files containing this outline. Among these files, this function outputs an altered nifti. This is the final file in the FSL pre-processing pipeline and is further converted to *.mat file for the tractography steps to be performed in ExploreDTI.

2. Tractography

Tractography of ICP was performed in ExploreDTI by the seed point propagation. The study performed by Leitner Y. et al was used as a reference for ICP segmentation [8]. Seed point placements were visual and did not involve clinical expertise upon placement. Two seed points were placed in a similar way as shown in Figure 2. However, the placement was compromised by the presence of a tumour and, therefore, different anatomical arrangements and symmetry of the cerebellar structures (Figure 5). Two additional AND ROIs were allocated at the approximate location of the ICP ending, which can be seen in Figure 6. This was done to exclusively investigate the segment of the ICP tracts. The FA and MD parameters were then outputted in the form of *.txt files. These could be used for further analysis to provide a more quantitative insight into the cerebellar structures, especially ICP.

Angle deviation and step size are parameters for tractography, which should be set to enable sufficient curvature of the tract while avoiding anatomically infeasible curvature. A smaller step size should be applied with the lower angle deviation threshold. Therefore, the step size should be smaller than a voxel size, with half a voxel size being a standard option. The seed point resolution has been chosen according to the voxel size. In this cohort, the voxel sizes are 2 – 2.3 mm. The default tractography algorithm was executed. Appendix C can be consulted for a review of the setting details.

The qualitative assessment of the data is visually performed on the residual maps (Figures 3, 10). These maps represent whether the diffusion data fits the estimated model well, where brighter colours highlight areas with higher deviation from the model. The model estimation approach of choice here was linear. Because it is the default setting in ExploreDTI and the focus of the project was to find out the pre-processing pipeline that gives the biggest improvements on a particular dataset, not many alterations were done with the choice of model estimation.

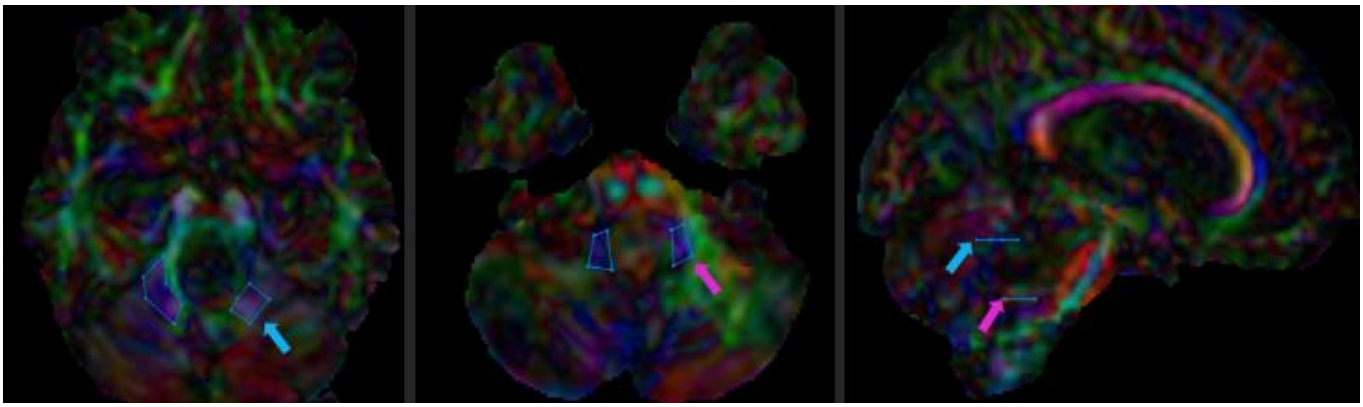

FIGURE 5. Seedpoint allocation for the segmentation of inferior cerebellar peduncle (ICP), following the reference by Leither et.al. [7]
Blue ROIs (regions of interest) are seedpoints (starting points in tract propagation).
Arrows are pointing at the seedpoint allocation for the right ICP.

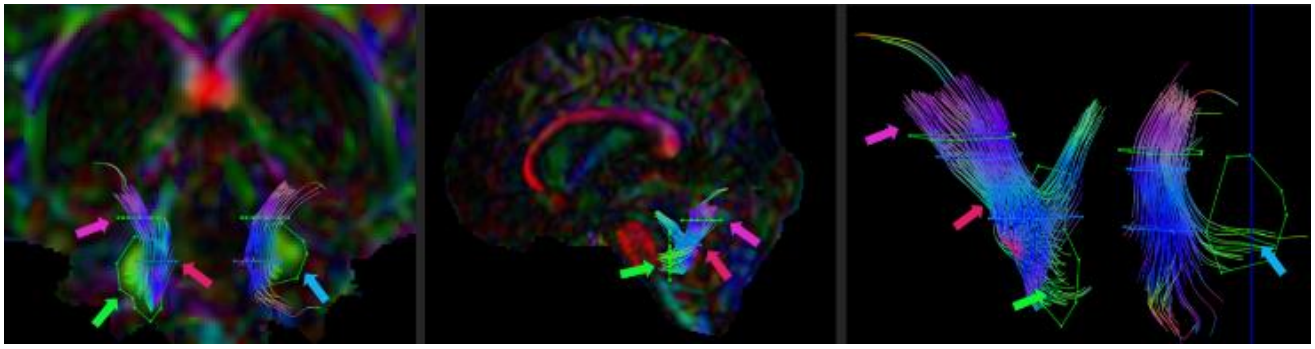

FIGURE 6. ROI (region of interest) placement, closeup. Blue ROIs are seedpoints (starting points in tract propagation). Green ROIs are AND ROIs (only the tracts passing through both AND ROI gates will be considered, the rest is ignored). Additional examples of ROI allocation and seedpoint propagation and tractography results can be found in Appendix D.

RESULTS

Pre-Processing

Figure 9 illustrates a step-by-step improvement with the use of FSL pre-processing method. Raw data has a noticeable amount of zig-zag patterns, which are common artefacts in sagittal and coronal views, especially when acquiring paediatric patient data. This was hypothesised to get solved with an application of *eddy* tool, which performs slice-to-volume movement correction. However, some of those artefacts are still present. Differences after application of *epi_reg* function are shown in Figures 9b and 9c. The distortion of remaining artefacts from 9b follows through the registration process. This is not ideal, however, in this pipeline, this function only performs image registration. So, the unresolved artefacts from Figure 9b remain in Figure 8c. The arrows are pointing at the most noticeable changes. The same volume has been visualised for every patient and follows through Figure 9a-9c.

From the Figures 7 and 8 it can be seen that FSL pipeline has an advantage over the outcomes from the ExploreDTI when resolving acquisition artefacts. A comparatively higher amount of remaining eddy current induced distortions is present in Figure 8, showing ExploreDTI outcomes. Blue and pink arrows point at the remaining acquisition artefacts, like eddy current induced image blurring, which remained in both cases. Green arrow points at the non-white matter tissues, which should have been excluded with an application of BET tool. Additional figures can be found in Appendix D.

From the comparison of residual maps in Figures 3 and 10, it can be seen that the high number of residuals is still present in the data. However, it is important to remember that no data is perfect, and residuals will be present in any case. So, the aim is to have some more or less uniformly distributed level of residuals present. In this cohort, some residuals in the cerebellar region are expected and acceptable due to the presence of a tumour. Potential improvements are mentioned in the discussion section.

Tractography

The presence of acquisition artefacts has an effect of interfering with tract propagation and segmentation and, therefore, decreasing the reliability of quantitatively acquired diffusion measures (FA, MD). The allocation of ROI was done as described by Y. Leither et.al. and is shown in Figures 2, 5, 6 [8]. Results of ICP segmentation are visualized in Figure 11. Further analysis of fiber bundle properties was not performed due to the large amount of inaccuracies supplied by the persisting acquisition artefacts. Statistical analysis of tract descriptive parameters was initially planned but got prematurely stopped and cancelled. Because the current method should undergo more development before quantitative tractography results can be reliable.

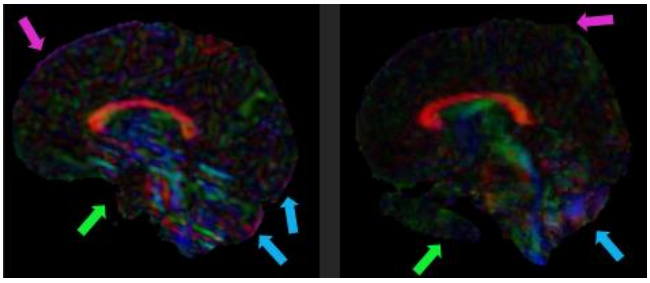

FIGURE 7. Results after the pre-processing pipeline in ExploreDTI visualised for 2 different patients, same as in Figure 8.

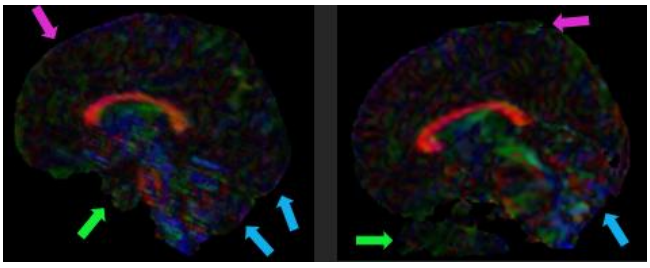

FIGURE 8. - Results after the pre-processing pipeline in FSL visualised for 2 different patients, same as in figure 7. In this figure blue and pink arrows point at the acquisition artefacts. Green arrows point at the BET tool related issues.

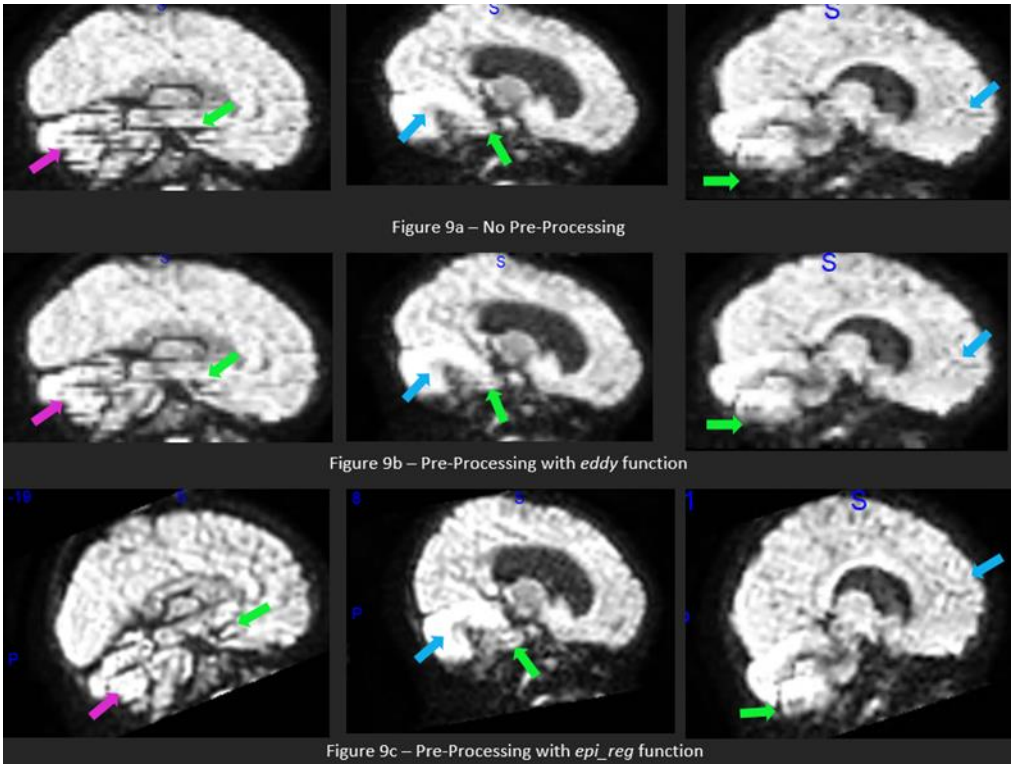

FIGURE 9. **Visualisation of the steps in FSL pre-processing pipeline. Top to bottom of each column – no pre-processing (9a), visualisation after the *eddy* function (9b), the result after the *epi_reg* function (9c).**
Three different patients have been visualised and the same volume has been illustrated for each patient throughout 9a, 9b, 9c. The arrows point at the noticeable artefacts.

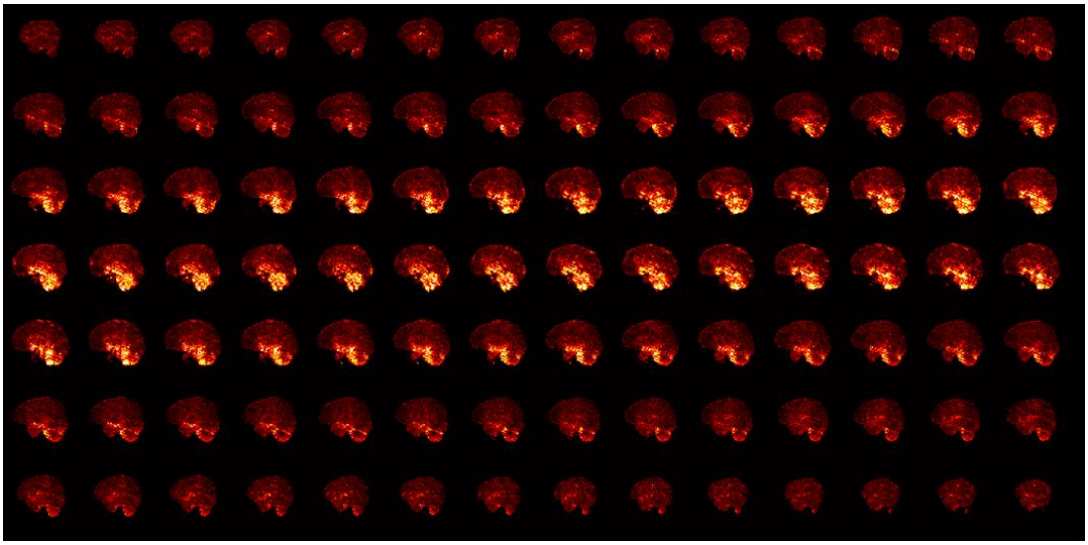

FIGURE 10. **Residual map after the FSL pre-processing pipeline. Yellow regions highlight differences between the model estimated values and the actual measurements. Same patient as in Figure 3.**

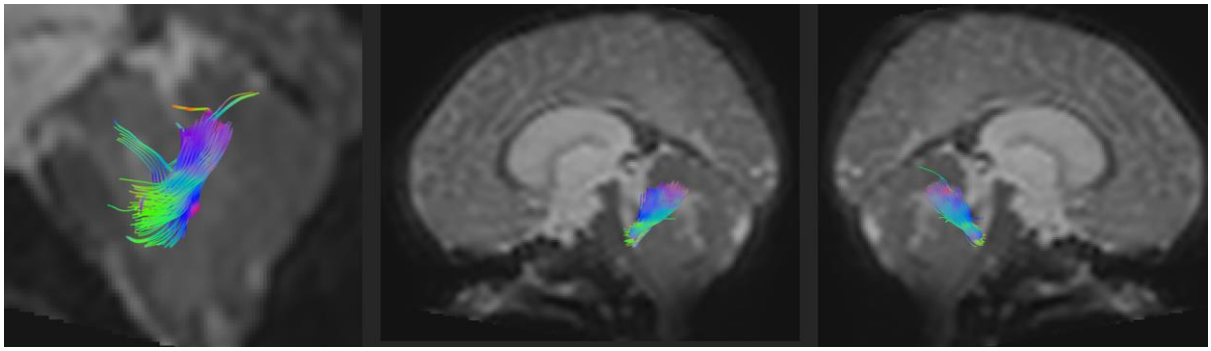

FIGURE 11. **Examples of ICP tract segmentation overlapped with T1-weighted volume. Visualisation is done for two different patients, where the second and third image belongs to the same patient. More examples are provided in the Appendix D.**

DISCUSSION AND A CONCLUSION

The project provides an overview of two different pre-processing pipelines (ExploreDTI and FSL) for paediatric data with posterior fossa tumours. An adequate pipeline has been exerted on 14 patient records, and then tractography of the inferior cerebellar peduncle was attempted. The data quality inspection was based on residual maps, visual comparison of the diffusion-weighted and T1-weighted MRI scans and tractography.

Main challenges, which should be taken into consideration for future investigation of the problem are:

- High anatomical variability of the cerebellar structures (natural and age-dependent)
- Presence of tumour, which leads to distortions and termination in tracts propagation
- High variance of tumours present (clinical diagnosis, allocation, diameter etc)
- Required experience in tumour delineation

The abovementioned factors introduce a considerable amount of variability, which makes it complicated to identify a quantitative marker. Inconsistent labelling in clinical records posed a larger challenge than expected with respect to the data pre-processing and analysis. Consistent labelling according to the golden standard protocols is important for the conduction of projects like this. The complexity of data is also dictated by different acquisition protocols and the number of post-surgical check-ups conducted. The total amount of scans in each patient folder varies, as do the parameters like single or multi-shell b-values.

The initial aim of quantifying the tract parameters, like FA and MD, after the ICP segmentation has underestimated some necessary prerequisite steps. Due to the lack of standardisation, it was decided to deal with samples acquired with a similar acquisition protocol. This has reduced the sample size from 148 to 36 and 14 for pre-processing and tractography, respectively. The study design, consisting of small sample size, shifted the focus of the project to a qualitative comparison of pre-processing techniques.

Qualitative evaluation of the results was primarily based on visual examination. Residual maps illustrate how well the estimated model fits the data (Figure 3, 10). In this pipeline, the classical approach of a linear model estimation was used. Changes related to the model estimation process can be detected by testing out other methods, while considering the given data. Here this could potentially be improved by the execution of REKINDLE (Robust Extraction of Kurtosis INDices with Linear Estimation) method, which would perform a robust model estimation with an application of RESTORE (Robust EStimation of Tensors by Outlier REjection) algorithm [28].

Finding a way to quantitatively assess the presence of residuals in data is necessary for future project development. However, the high number of residuals in the cerebellar region here does not necessarily indicate inadequate model fit. This part of the brain is generally associated with a higher number of visualisation challenges, because dMRI data is sensitive to pulsatile microscopic movements and patient motion and cerebellum is an anatomically dense area. The obstruction of the brain with the occurrence of the tumour contributes to the diffusion data analysis process being troublesome. It is hard to know if residuals arise from the tumour pathophysiology, gradient instability, errors in registration or model estimation. The advancement of acquisition protocols could improve the chances of solving this issue. A better insight into the quality of residuals present can also be provided with a tumour segmentation algorithm applied to residual maps. For example, by creating a tumour mask and then excluding that region from the residual map, a better comparison of the artefacts outside that region can be investigated.

Another detail is the presence of acquisition artefacts, which are likely to persist even with the expansion of acquisition protocol. Like the zig-zag pattern, typical for paediatric patient's scans, which is visible in Figure 3. Even though FSL

pipeline resulted in more visual improvement compared to ExploreDTI pre-processing, not all artefacts were eliminated. This proves that more alterations to the pre-processing pipeline, or a change for the future acquisition protocols, are necessary. The assumption held by the corrective algorithm is a stillness of a patient in the scanner in between the volume acquisitions. However, that is hardly ever true in the case with paediatric patients (usually happens due to the patient movement). This was hypothesised to be corrected with the slice-to-volume registration option in *eddy* tool. Even though eddy current correction in FSL has improved overall quality, artefacts are still present in some of the volumes. This can be because of an insufficient number of directions corresponding to the b-value. Higher b-values require a bigger number of directions, here it is 17 on 1000 s/mm^2 and 16 on 800 s/mm^2 volumes and b-values respectively. A recommended proportion is b-value of 1500 and 10-15 directions. More recommendations on the improvement of the acquisition for the purposes of eddy correction are listed in the manual, which should be consulted for future improvements of the pre-processing pipeline [29].

Some of the pre-processing FSL tools allow for expanded functionality by setting additional parameters. To improve the outcomes, a good example is to add some parameters into *eddy*. In the applied pipeline, pseudo files with acquisition parameters were created. Access to the real acquisition parameters would be highly beneficial. With this information, the execution of eddy current induced distortions correction function in the described pipeline can be advanced. It could split the correction into two steps: fix susceptibility-induced distortions with the *topup* function first and then supplying the results to *eddy* for a better correction. The *topup* function requires at least two varying acquisition parameters, the two with opposing phase-encoding polarities would suffice. It calculates the eddy current-related off-resonance field and susceptibility-induced off-resonance field. The current cohort did not contain this information, so the acquisition parameters text file was filled with the approximate numbers. It did not cause additional variations in the cohort since those 14 patients have been scanned with the same protocol. This addition would also make it possible to perform registration and EPI distortion correction with the use of *epi_reg* function, which would, potentially, speed up the overall pre-processing.
Obtaining data in future with different and more expansive acquisition protocols could also give more freedom in the choice of tractography methods. For example, acquiring data with at least one more b-value setting would allow performing diffusion kurtosis imaging (DKI), which is more robust but also computationally expensive [30]. Another problem to consider is a fiber bundle crossing. That cannot be tackled with the current acquisition protocol and can lead to errors in tractography. Resolving the issue of inter-voxel crossing fibers would result in more reliable fiber tract estimation and better segmentation of the tracts of interest [31]. This issue arises due to a computational power limitation – the size of the voxel does not precisely represent anatomical arrangement within the visualised area. Advancing acquisition protocols could potentially solve this limitation. Improvements in the acquisition protocols could make it possible to investigate patient data with the diffusion imaging methods that allow a higher focus on the details. For example, acquiring diffusion data with HARDI (High Angular Resolution Diffusion Imaging) would be beneficial to gain more precision in resolving fiber bundle angulation [32]. Because, after all, the tractography is based on a diffusion model estimation. And the best improvements can be achieved by making sure more data with higher accuracy and precision is acquired. The disadvantage is that every addition makes the acquisition time longer. For example, the scanning time increases proportionally to the number of EPI shots [33]. Associated complications also include that it is a paediatric cohort and hence time in the scanner should be minimised. It also should be shortened due to practical reasons related to hospital management.

Additionally, the seed point allocation could use some improvement in its anatomical planning. Having educated guesses from clinical perspective on the anatomical outcomes of the fiber-tracking could also be beneficial. An experienced radiologist or a well-trained AI algorithm would increase the precision and accuracy of the segmentation. If that option is possible, spending more time on tuning the tractography parameters would be a worthwhile next step. Knowing the anatomical composition of the cerebellar peduncle of interest would help altering the tractography parameters accordingly to the expected curvature of the tracts, like angle threshold and fiber length. Using the previous anatomical knowledge, you can also define the range of the pathways. This would allow stopping tracts' propagation if the fibre length exceeds the anatomically expected one or only allowing tracts whose angle threshold does not exceed a set angular threshold value. Because diffusion imaging works best if you know what you are looking for. Also, by increasing the seed point resolution (e.g. from 2x2x2 to 1x1x1 voxels) the algorithm would take smaller processing steps. However, that would result in a higher computational complexity, processing time and an increase in required storage space.

Once the pre-processing and tractography pipelines are improved, the quantification of FA and MD values can be done. This would allow to compare tract profile characteristics. This stage would require an evaluation step and that could be done with an allocation of a fixed number of equidistant points along the tracts. This is a better measure of tract properties than averaging because at different points along the tracts it can naturally exhibit different properties (curvature, angle deviation, stepsize etc).

Additionally, identification of the optimal dMRI data processing and statistical evaluation methods is associated with the following challenges: scans of patients of different ages are collected within the dataset. This would mean different sizes of the brain and the shape of the brain structures. From a clinical perspective, this also means a different surgical approach, which leads to different pre- and post-operational procedures, presence of edema and changed anatomy. Therefore, having sufficient clinical expertise is important in the investigation of this research topic. An investigation of differences in several brain tumour types, as well as the identification of the type of reaction happening in damaged brain structures is a potential extension of the current topic.

While working with paediatric and adolescent data we need to also consider regional brain ageing and development. The age variability between the patients contributes to unreliability, which is conditioned by the fact that brain development does not happen linearly in different brain parts. Learning about stages and patterns in brain development and how that corresponds to the age of the patients from cohort should be considered when trying to answer similar research questions. When trying to understand why some patients develop syndrome and others do not, both a CMS and non-CMS groups are required. Unfortunately, this cohort of 14 patients contained only two samples, one per gender group, who had developed CMS.

In conclusion, the FSL pre-processing method has resulted in more visual improvements, compared to ExploreDTI. However, not all artefacts were eliminated. The presence of acquisition artefacts has an effect of interfering with tract propagation and segmentation and, therefore, decreasing the reliability of quantitative measures. The current method should therefore undergo more development before tractography results can be reliably quantified. Overall, an acquisition protocol obtaining multiple b-values and increasing the total number of diffusion directions would give flexibility of choice when testing which processing pipeline suits the research question best. The benefits of keeping track of acquisition parameters in terms of pre-processing were also mentioned. The complexity of the research question requires a more circumstantiated individual evaluation of steps and the data in order to answer why do some patients develop cerebellar mutism syndrome, while others do not.

REFERENCES

[1] Pitsika M, Tsitouras V. Cerebellar mutism. Journal of Neurosurgery: Pediatrics. 2013;12(6):604-614.

[2] van Baarsen K, Grotenhuis J. The anatomical substrate of cerebellar mutism. Medical Hypotheses. 2014;82(6):774-780.

[3] van Baarsen K, Kleinnijenhuis M, Konert T, van Cappellen van Walsum A, Grotenhuis A. Tractography Demonstrates Dentate-rubro-thalamic Tract Disruption in an Adult with Cerebellar Mutism. The Cerebellum. 2013;12(5):617-622.

[4] D'Angelo E, Mazzarello P, Prestori F, Mapelli J, Solinas S, Lombardo P et al. The cerebellar network: From structure to function and dynamics. Brain Research Reviews. 2011;66(1-2):5-15.

[5] Middle cerebellar peduncle image - Wikipedia [Internet]. En.wikipedia.org. 2022. Available from: https://en.wikipedia.org/wiki/Middle_cerebellar_peduncle

[6] Grønbæk J, Wibroe M, Toescu S, Frič R, Møller L, Grillner P et al. Postoperative Speech Impairment and Surgical Approach to Posterior Fossa Tumours in Children: A Prospective European Multicentre Study. SSRN Electronic Journal. 2021;.

[7] De Smet H, Baillieux H, Catsman-Berrevoets C, De Deyn P, Mariën P, Paquier P. Postoperative motor speech production in children with the syndrome of 'cerebellar' mutism and subsequent dysarthria: A critical review of the literature. European Journal of Paediatric Neurology. 2007;11(4):193-207.

[8] Leitner Y, Travis K, Ben-Shachar M, Yeom K, Feldman H. Tract Profiles of the Cerebellar White Matter Pathways in Children and Adolescents. The Cerebellum. 2015;14(6):613-623.

[9] Soelva V, Hernáiz Driever P, Abbushi A, Rueckriegel S, Bruhn H, Eisner W et al. Fronto-cerebellar fiber tractography in pediatric patients following posterior fossa tumor surgery. Child's Nervous System. 2012;29(4):597-607.

[10] Liu C, Williams K, Orr H, Akkin T. Visualizing and mapping the cerebellum with serial optical coherence scanner. Neurophotonics. 2016;4(01):1.

[11] Mariën P, Beaton A. The enigmatic linguistic cerebellum: clinical relevance and unanswered questions on nonmotor speech and language deficits in cerebellar disorders. Cerebellum & Ataxias. 2014;1(1).

[12] Catsman-Berrevoets C. Cerebellar mutism syndrome: cause and rehabilitation. Current Opinion in Neurology. 2017;30(2):133-139.

[13] Weinstein, D.; Kindlmann, G.; Lundberg, E.:Tensorlines. Advection-Diffusion based Propagation through Diffusion Tensor Fields, Center for Scientific Computing and Imaging, Department of Computer Science, University of Utah. Proceedings of the conference on Visualization '99.

[14] Nimsky C, Ganslandt O, Hastreiter P, Wang R, Benner T, Sorensen AG, Fahlbusch R. Preoperative and intraoperative diffusion tensor imaging-based fiber tracking in glioma surgery, Neurosurgery, Vol.56(1): 130-7, 2005.

[15] NITRC: MRIcron: Tool/Resource Filelist [Internet]. Nitrc.org. 2022 [cited 25 July 2022]. Available from: https://www.nitrc.org/frs/?group_id=152

[16] Leemans A, Jeurissen B, Sijbers J, and Jones DK. ExploreDTI: a graphical toolbox for processing, analyzing, and visualizing diffusion MR data. In: 17th Annual Meeting of Intl Soc Mag Reson Med, p. 3537, Hawaii, USA, 2009"

[17] Vos S, Tax C, Luijten P, Ourselin S, Leemans A, Froeling M. The importance of correcting for signal drift in diffusion MRI. Magnetic Resonance in Medicine. 2016;77(1):285-299.

[18] Jesper L. R. Andersson, Mark S. Graham, Ivana Drobnjak, Hui Zhang, Nicola Filippini and Matteo Bastiani. Towards a comprehensive framework for movement and distortion correction of diffusion MR images: Within volume movement. NeuroImage, 152:450-466, 2017.

[19] Leemans A, Jones D. TheB-matrix must be rotated when correcting for subject motion in DTI data. Magnetic Resonance in Medicine. 2009;61(6):1336-1349.
[20] Jeurissen B, Leemans A, Sijbers J. Automated correction of improperly rotated diffusion gradient orientations in diffusion weighted MRI. Medical Image Analysis. 2014;18(7):953-962.
[21] Tax C, Bastiani M, Veraart J, Garyfallidis E, Okan Irfanoglu M. What's new and what's next in diffusion MRI preprocessing. NeuroImage. 2022;249:118830.
[22] Jesper L. R. Andersson, Mark S. Graham, Ivana Drobnjak, Hui Zhang, Nicola Filippini and Matteo Bastiani. Towards a comprehensive framework for movement and distortion correction of diffusion MR images: Within volume movement. NeuroImage, 152:450-466, 2017.
[23] eddy/UsersGuide - FslWiki [Internet]. Fsl.fmrib.ox.ac.uk. 2022 [cited 2 July 2022]. Available from: https://fsl.fmrib.ox.ac.uk/fsl/fslwiki/eddy/UsersGuide
[24] Jesper L. R. Andersson, Mark S. Graham, Ivana Drobnjak, Hui Zhang, Nicola Filippini and Matteo Bastiani. Towards a comprehensive framework for movement and distortion correction of diffusion MR images: Within volume movement. NeuroImage, 152:450-466, 2017.
[25] Jeurissen B, Leemans A, Sijbers J. Automated correction of improperly rotated diffusion gradient orientations in diffusion weighted MRI. Medical Image Analysis. 2014;18(7):953-962.
[26] Jesper L. R. Andersson, Mark S. Graham, Eniko Zsoldos and Stamatios N. Sotiropoulos. Incorporating outlier detection and replacement into a non-parametric framework for movement and distortion correction of diffusion MR images. NeuroImage, 141:556-572, 2016.
[27] FslOverview - FslWiki [Internet]. Fsl.fmrib.ox.ac.uk. 2022 [cited 25 July 2022]. Available from: https://fsl.fmrib.ox.ac.uk/fsl/fslwiki/FslOverview
[28] Tax C, Otte W, Viergever M, Dijkhuizen R, Leemans A. REKINDLE: Robust extraction of kurtosis INDices with linear estimation. Magnetic Resonance in Medicine. 2014;73(2):794-808.
[29] Jeurissen B, Leemans A, Sijbers J. Automated correction of improperly rotated diffusion gradient orientations in diffusion weighted MRI. Medical Image Analysis. 2014;18(7):953-962.
[30] Van Cauter S, De Keyzer F, Sima D, Croitor Sava A, D'Arco F, Veraart J et al. Integrating diffusion kurtosis imaging, dynamic susceptibility-weighted contrast-enhanced MRI, and short echo time chemical shift imaging for grading gliomas. Neuro-Oncology. 2014;16(7):1010-1021.
[31] Landman B, Bogovic J, Wan H, ElShahaby F, Bazin P, Prince J. Resolution of crossing fibers with constrained compressed sensing using diffusion tensor MRI. NeuroImage. 2012;59(3):2175-2186.
[32] Descoteaux M. High Angular Resolution Diffusion Imaging (HARDI). Wiley Encyclopedia of Electrical and Electronics Engineering. :1-25.
[33] Luna A, Ribes R, Soto J. Diffusion MRI outside the brain. Heidelberg: Springer-Verlag Berlin Heidelberg; 2012.
[34] Giannelli M, Cosottini M, Michelassi M, Lazzarotti G, Belmonte G, Bartolozzi C et al. Dependence of brain DTI maps of fractional anisotropy and mean diffusivity on the number of diffusion weighting directions. Journal of Applied Clinical Medical Physics. 2009;11(1):176-190.

Appendix A – Background information on physics of dMRI

The diffusion MR imaging (dMRI) technique is based on the principle of molecular diffusivity. Particularly the Brownian motion, which is a constant random motion of the molecules in free water.
Tissues are distinguishable on the MRI scans due to the differences in relaxation rates. The differences in water molecule magnetisation can be overlapped with MRI scan, which is used as a reference for diffusion data registration.
The dMRI approach can provide an overview of the volumetric white matter (WM) microstructural changes by estimating the model of the predominant movement of water molecules in the brain [33]. Different tissue types have different corresponding diffusion coefficients. Fractional anisotropy (FA) is a microstructural indicator of the strength of the predominant molecular diffusivity direction in the WM. It characterises the degree of diffusivity, where 0 would mean the isotropic diffusion, which is totally random, not constricted and has the same diffusion coefficient in all directions. The coefficient of anisotropic diffusion varies due to the differences in density of tissue types and water content. Grey matter generally has a higher FA, than white matter, while cerebrospinal fluid has a lower FA. WM tractography provides more certainty due to the more coherently aligned pathways and comparatively stronger defined tract profiles. In tractography, when adjusting tract propagation settings, the FA value is altered depending on the research goal. Here the default of 0.2 was used. With the higher FA we would have a higher certainty of the tract being there, however, this way there will be fewer tracts detected. Typically, FA values below 0.2 would show "phantom tracts", which are not WM but rather a cerebrospinal fluid. Grey matter generally has a higher FA value than white matter. So changing tractography settings, in that case, would result in propagation of fewer tracts, potential data loss or detection of grey matter instead of WM.

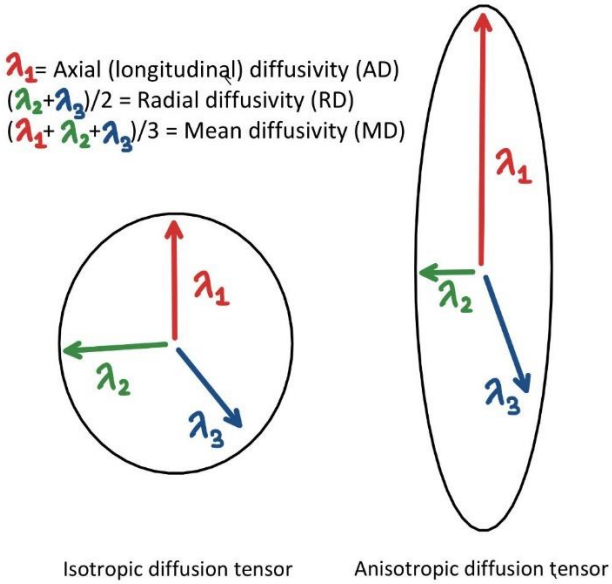

FIGURE A1. - Diffusion tensor shape examples, where λ1, λ2 and λ3 represent three main eigenvalues of a tensor. λ1 represents axial diffusivity (AD), mean of λ2 and λ3 corresponds to radial diffusivity (RD) and mean diffusivity (MD) consists of λ1, λ2 and λ3.

Quantification of the diffusion tensor model in best described by four measures: FA, mean diffusivity (MD), radial diffusivity (RD), and axial diffusivity (AD). MD is the descriptive measure derived from hindered diffusion data, which is an average value obtained from AD and RD. AD corresponds to the predominant tensor direction, while RD describes mean of second and third diffusion tensor eigenvalues (Figure 1).

Appendix B - Commands and settings for performance of FSL pre-processing pipeline:

An example of eddy tool setting, which was used as a part of the FSL pre-processing pipeline.

eddy --imain=108.nii.gz --mask=108_bet045.nii.gz --index=index.txt --acqp=acqp2.txt --bvecs=108_bvec.bvec --bvals=108_bval.bval --niter=8 --fwhm=10,8,4,2,0,0,0,0 --repol --out=108_eddy --mporder=2 –slspec=my_slspec.txt –s2v_niter=5 --s2v_lambda=1 --s2v_interp=trilinear --data_is_shelled

It is needed to additionally create the following files for EDDY function execution:

acqp2.txt – the text file containing acquisition parameters
index.txt – the text file corresponding to the total number of diffusion volumes
my_slspec.txt – the text file that contains information about slice or multi-band group acquisition. Should be created based on the z-dimension. Numbering goes from 0 to the maximum even number and then from 1 to the maximum odd number in your data.

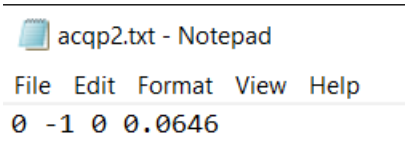

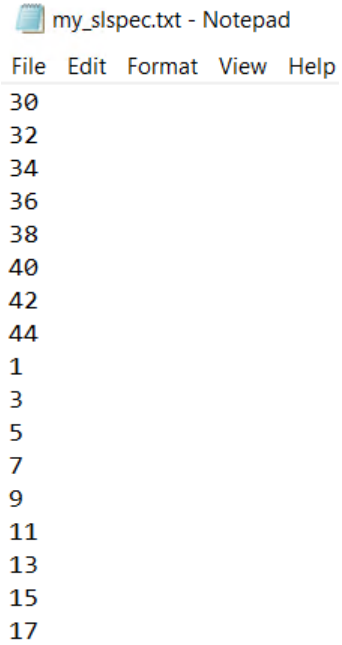

All the following functions were performed on the example file number 108.

Changes in the nomenclatures are corresponding to the default ones by FSL.

For more information, refer to the FSL user guide [19].

EPI_REG

epi_reg --epi=108 --t1=108_T1w_crop --t1brain=108_T1w_crop_bet045 --out=108_epi_reg

Appendix C - Applied tractography settings:

Minimal FA for seed point selection [0,1]
0.2

Maximal FA for seed point selection [0,1]
1

Minimal FA to allow tracking [0,1]
0.2

Maximal angle [0,90]
30

Step size (in mm)
1

Minimal fiber length (in mm)
1

Maximal fiber length (in mm)
500

Seedpoint super sampling factor
[0 0 0]

Appendix D – Additional Tractography Results

Segmentation of inferior cerebellar peduncle (ICP) performed after FSL pre-processing pipeline.

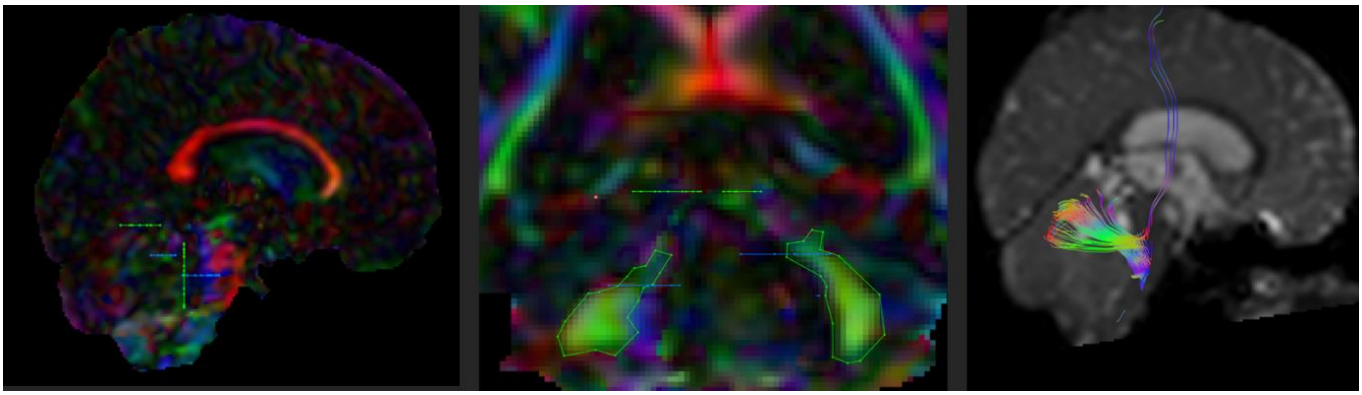

FIGURE D1. - ROI (region of interest) placement, closeup. Blue ROIs are seedpoints (starting points in tract propagation).
Green ROIs are AND ROIs (only the tracts passing through both AND ROI gates will be considered, the rest is ignored).

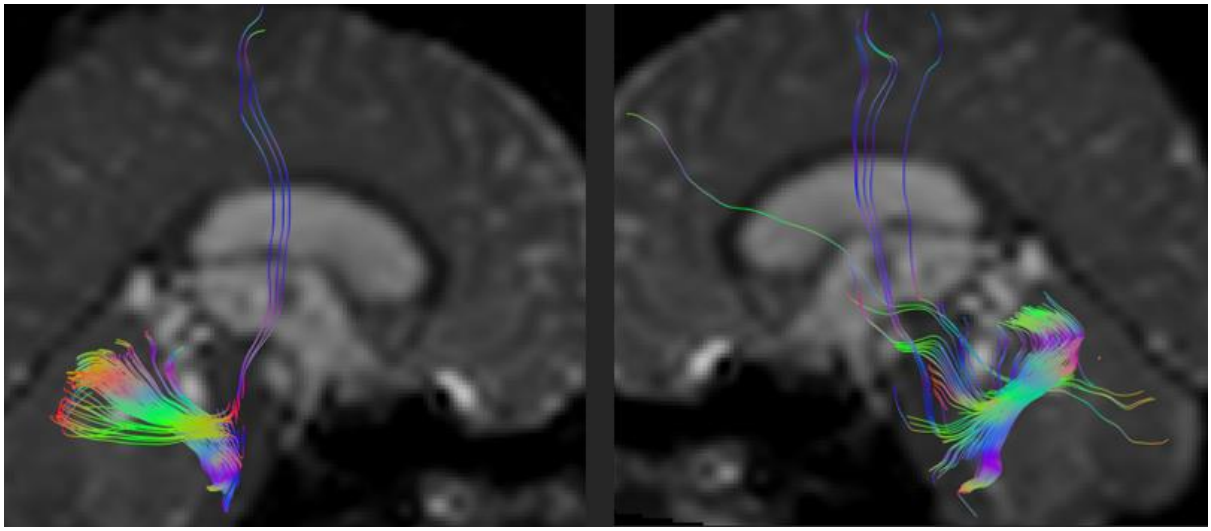

FIGURE D2. – Left and right ICP segmentation in the same patient after the pre-processing in FSL.

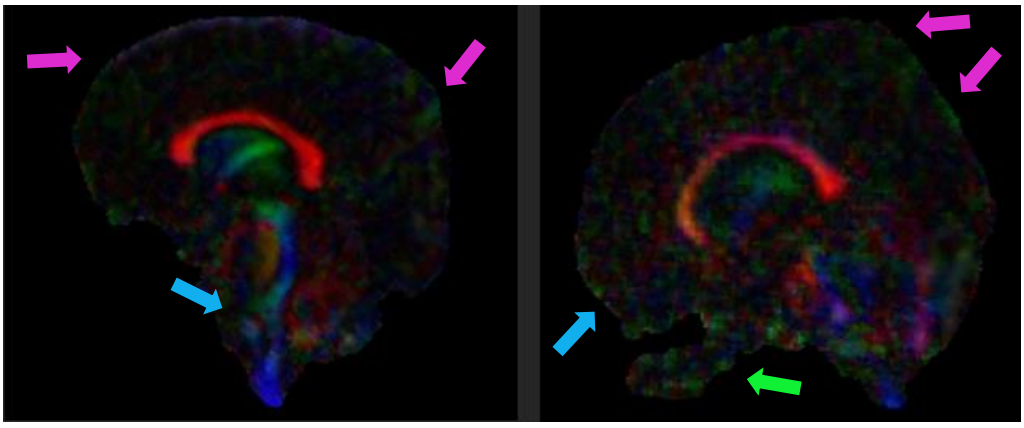

FIGURE D4A. – Additional results after the pre-processing pipeline in ExploreDTI visualised for 2 different patients.
In this figure blue and pink arrows point at the acquisition artefacts. Green arrows point at the BET tool related issues.

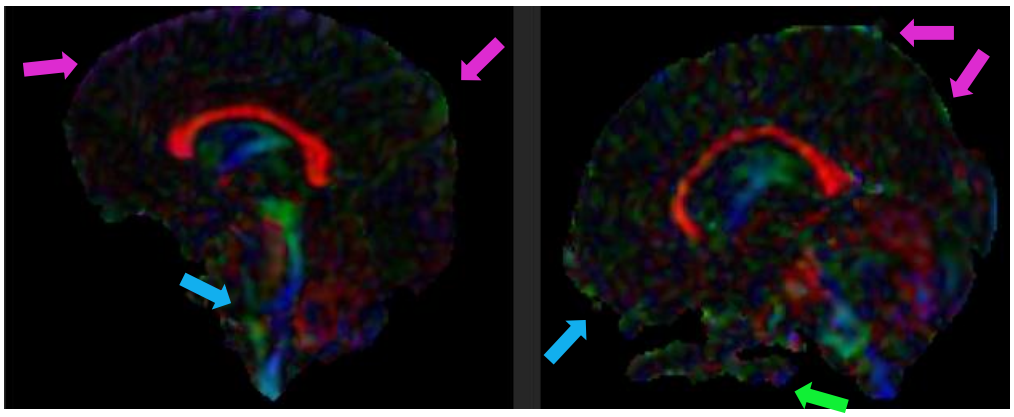

FIGURE D4B. – Additional results after the pre-processing pipeline in FSL visualised for 2 different patients.
In this figure blue and pink arrows point at the acquisition artefacts. Green arrows point at the BET tool related issues.

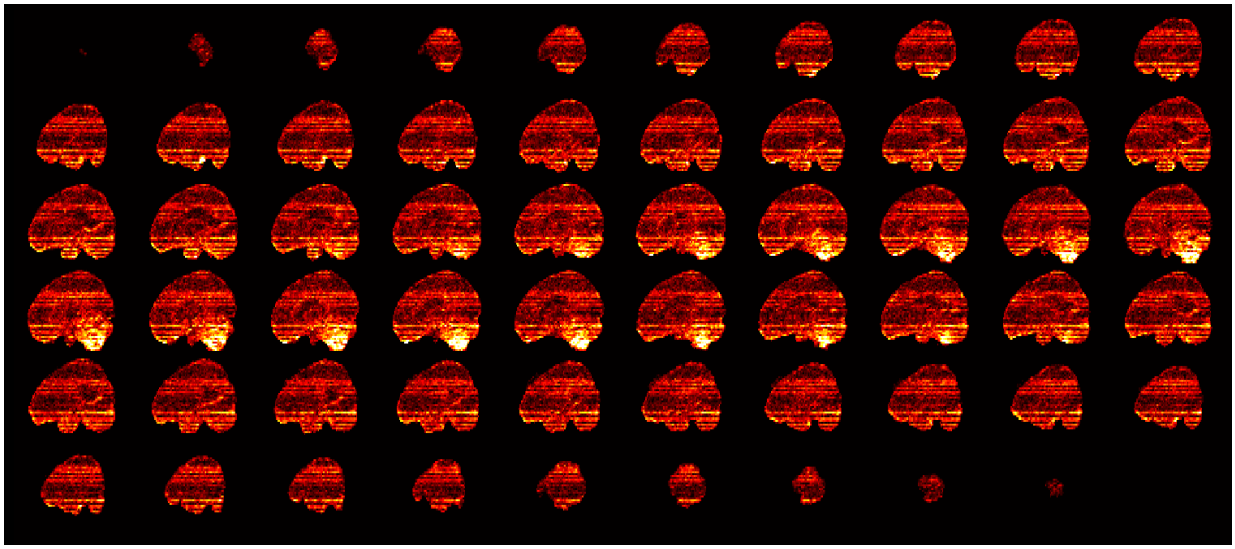

FIGURE D5A. – Additional residual maps. No Pre-Processing.

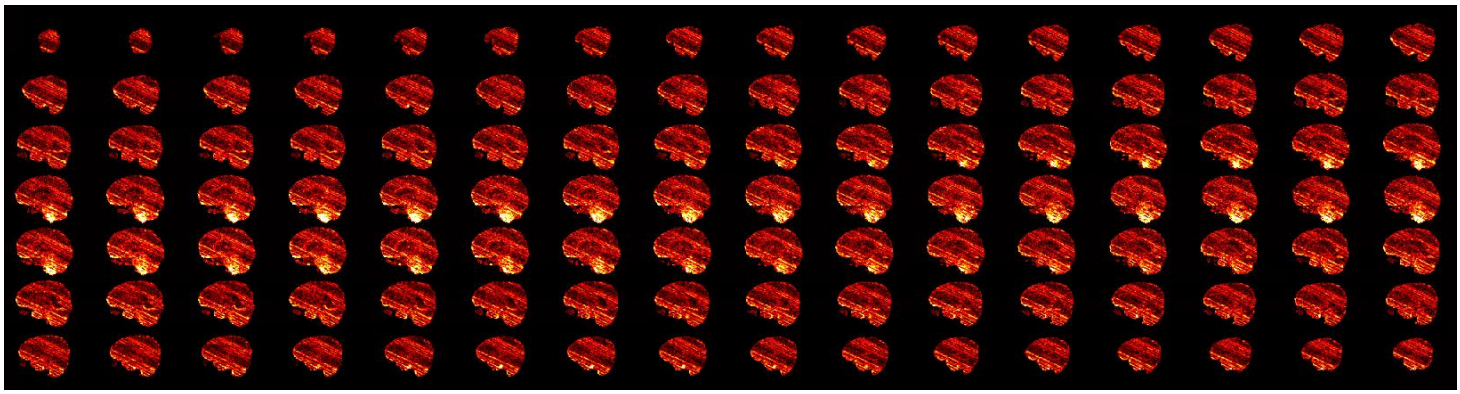

FIGURE D5B. – Additional residual maps. After FSL Pre-Processing.